JACS
JOURNAL OF THE AMERICAN CHEMICAL SOCIETY

Article

pubs.acs.org/JACS

Solution-Phase Monitoring of the Structural Evolution of a Molybdenum Blue Nanoring

Haralampos N. Miras, Craig J. Richmond, De-Liang Long, and Leroy Cronin*

School of Chemistry, WestCHEM, The University of Glasgow, Glasgow G12 8QQ, United Kingdom

Supporting Information

ABSTRACT: The inorganic host–guest complex $Na_{22}\{[Mo^{VI}_{36}O_{112}(H_2O)_{16}]\subset[Mo^{VI}_{130}Mo^{V}_{20}O_{442}(OH)_{10}(H_2O)_{61}]\}\cdot 180H_2O \equiv \{Mo_{36}\}\subset\{Mo_{150}\}$, compound **1**, has been isolated in its solid crystalline state via unconventional synthesis in a custom flow reactor. Carrying out the reaction under controlled flow conditions selected for the generation of $\{Mo_{36}\}\subset\{Mo_{150}\}$ as the major product, allowing it to be reproducibly isolated in a moderate yield, as opposed to traditional "one-pot" batch syntheses that typically lead to crystallization of the $\{Mo_{36}\}$ and $\{Mo_{150}\}$ species separately. Structural and spectroscopic studies of compound **1** and the archetypal Molybdenum Blue (MB) wheel, $\{Mo_{150}\}$, identified compound **1** as a likely intermediate in the $\{Mo_{36}\}$ templated synthesis of MB wheels. Further evidence illustrating the template effect of $\{Mo_{36}\}$ to MB wheel synthesis was indicated by an increase in the yield and rate of production of $\{Mo_{150}\}$ as a direct result of the addition of preformed $\{Mo_{36}\}$ to the reaction mixture. Dynamic light scattering (DLS) techniques were also used to corroborate the mechanism of formation of the MB wheels through observation of the individual cluster species in solution. DLS measurement of the reaction solutions from which $\{Mo_{36}\}$ and $\{Mo_{150}\}$ crystallized gave particle size distribution curves averaging 1.9 and 3.9 nm, consistent with the dimensions of the discrete clusters, which allowed the use of size as a possible distinguishing feature of these key species in the reduced acidified molybdate solutions and to observe the templation of the MB wheel by $\{Mo_{36}\}$ directly.

INTRODUCTION

The term "self-assembly" is often used as an all-encompassing explanation to rationalize the formation of very large molecules and supramolecular aggregates, but unfortunately this term lacks specific mechanistic details.[1] These details could be very important in the ongoing efforts to understand, control, predict, and then design multifunctional inorganic materials by use of molecular synthons, which exhibit well-defined structure and linkable geometries.[2] Furthermore, the prediction of the observed properties of nanosized materials,[3] such as porosity (well-defined cavities or channels),[4] electronic and ionic transport,[5] magnetism,[6] luminescence,[7] and catalytic activity,[8] are among the most challenging problems in modern materials chemistry. Research into the design and application of metal organic frameworks (MOFs) or coordination polymers (CPs) has benefited greatly from successfully overcoming some of these problems by drawing such links between the predicted and experimentally determined properties. The knowledge of metal coordination geometries combined with organic linker lengths and geometries creates almost limitless possibilities for generating preconceived architectures such as macrocycles,[9] cages,[10−12] interlinked knots and helices,[13−15] and extended 3D frameworks.[16,17] Achieving this level of control via a "bottom-up" approach for the synthesis of larger inorganic functional nanosized architectures (2−10 nm), such as metallic nanoparticles and quantum dots, is, however, still a challenging prospect.[18−21] Polyoxometalates are solution-processable molecular metal oxides with structures of nanoscale dimensions; they range in sizes from 0.5 nm for the $\{Mo_6\}$ Lindquist to 5.3 nm for the gigantic $\{Mo_{368}\}$ giant "blue lemon" cluster, which is comparable to some small proteins in terms of molecular dimensions.[22,23] Polyoxometalates, with their facile one-pot syntheses,[24] unusually high conductivity, wide ranges of composition, size, and architecture,[25−27] and their ability to stabilize transition metal-based cores,[28,29] therefore play an important role in the discovery of new nanoscale materials and technologies from bottom-up strategies.[30−32] In our own work in this area, we have been working on a general approach to screen the assembly of polyoxometalates using a range of approaches,[33] most notably with electrospray mass spectrometry.[34]

The $\{Mo_{368}\}$ cluster mentioned previously belongs to the Molybdenum Blue (MB) polyoxometalate structure subset, so-called because of the intense blue color of their solutions.[35] This family (over 25 different species) of intensely colored, mixed-valence transition metal oxides includes a number of ring-shaped and spherical structures, namely, the MB rings[36−39] and Keplerates[40,41] respectively, which are formed by partial reduction of acidified molybdate solutions. These structures all share a key topological feature in the form of pentagonal $\{(Mo)Mo_5\}$ building units, which are essential for the formation of the resultant curved structures,[42] similar to the C_5 pentagons found in C_{60} buckminsterfullerene.[43] The presence of convex building blocks such as the pentagonal

Received: November 6, 2011
Published: January 17, 2012

   dx.doi.org/10.1021/ja210206z | J. Am. Chem. Soc. 2012, 134, 3816−3824

{(Mo)Mo_5} building units is intriguing and has caused a great deal of discussion regarding the nature of the discrete species available in the reaction mixture, as well as discussion regarding the mechanism of self-assembly. The key limitation with these discussions lies in the difficulty of characterizing the solution phase during the reaction, the identification of reaction intermediates, byproduct, as well as the product distribution and structural analysis. Unfortunately, the identification of individual metal−ligand complexes and clusters in such complex mixtures is an extremely difficult problem for polyoxometalate chemists as current solution-based techniques are limited in their application within this area. For example, NMR spectroscopy is hindered by the high levels of molecular/cluster symmetry and poorly receptive and often paramagnetic and labile metal nuclei. When used together, other spectroscopic techniques such as Raman, UV−vis, and IR spectroscopy can provide structural and electronic information for the bulk solution but offer little information on the identity of the individual building blocks. High resolution time-of-flight (TOF) and cryospray ionization mass spectrometry (CSI-MS),[44] dynamic light scattering (DLS),[45] and analytical ultracentrifugation (AUC)[46] have had greater levels of success in distinguishing between species in solution directly and have been used in conjunction with further evidence to formulate hypotheses on the assembly and disassembly processes of polyoxometalates.

It has been demonstrated that if an aqueous solution of sodium molybdate is acidified and reduced at room temperature, pure crystalline material containing {Mo_{154}}-type anions[47] can be obtained in high yield (several compounds with linked units (1D and 2D type) are also known).[36b] The intricate structure of these discrete {Mo_{154}} clusters can be described as follows: Each of the ring-shaped cluster fragments of the MB ring comprises 14 {Mo_8} units linked by 14 {Mo_1} and 14 {Mo_2} type units, $[\{Mo^{VI}_2O_5(H_2O)_2\}^{2+}_{b-x}(\{Mo^{VI/V}_8O_{26}(\mu_3\text{-}O)_2H_m\text{-}(H_2O)_3Mo^{VI/V}\}^{(4-m)-})_b]^{(2b-bm+2x)-}$ = $[\{Mo_2\}_{b-x}\text{-}\{Mo_8\}_b\{Mo_1\}_b]^{(2b-bm-2x)-}$; the {$Mo_8$} units, which occur in several polyoxomolybdates, can be considered as the fundamental building units of the ring structure, although a more general formulation discusses {Mo_{11}} units to unify the structural discussion of both the {Mo_{154}} wheel and {Mo_{132}} ball families.[47,48]

In the case of MB ring formation, ring size has been shown to be controllable by adjustment of the pH and reducing environment under which they form, where {Mo_{154}} = {Mo_{11}} × 14 is available between pH 1 and 2 and {Mo_{176}} = {Mo_{11}} × 16 becomes available at very low pH.[47b,48] In nonreduced molybdate solutions at pH ≈ 1.7, the dominant species is the isopolymolybdate $[Mo_{36}O_{112}(H_2O)_{16}]^{8-}$ ({Mo_{36}}), as identified by X-ray studies and other spectroscopic techniques[47] (Figure 1). These {Mo_{36}} units consist of two $\{Mo^{VI}_{17}O_{54}(H_2O)_8\}^{6-}$ ({Mo_{17}}) units stabilized by protonation and two $\{MoO_2\}^{2+}$ groups acting as linkers. The {Mo_{17}} units can be described as being made up of two $\{Mo^{VI}_8O_{27}(H_2O)_4\}$ ({Mo_8}) units fused via a {Mo_1} unit at the center of inversion. When these solutions are reduced, the {Mo_8} units gain electrons and therefore realign to compensate for the increased electrostatic repulsion, constructing a curvature of {Mo_8} units and eventually resulting in the formation of MB rings. The role of the {Mo_{36}} was therefore originally perceived to be a source of {Mo_8} building units that could be reduced and reassembled into the MB rings. However, in our recent work we have showed that the role of the {Mo_{36}} may be more important than just a simple internal feedstock and is in fact a crucial template around which the MB ring structures form.[49] To accomplish this, we employed flow conditions as a new synthetic approach for these systems, (Figure 2) whereby real-time adjustment of the experimental variables that trigger and direct the self-assembly process was achieved. In doing so, a 20-electron-reduced intermediate host−guest species, $Na_{22}\{[Mo^{VI}_{36}O_{112}(H_2O)_{16}]\subset[Mo^{VI}_{130}Mo^{V}_{20}O_{442}\text{-}(OH)_{10}(H_2O)_{61}]\}\cdot 180H_2O$ **1**, was trapped in its crystalline state, isolated, and characterized by single-crystal X-ray diffraction studies.

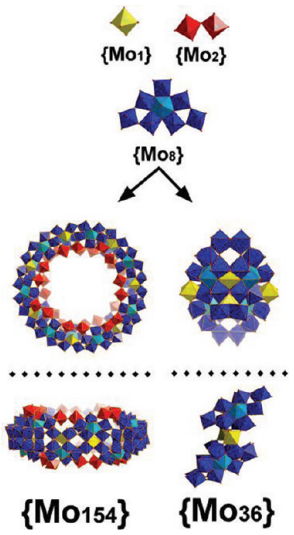

Figure 1. Scheme showing the assembly of the parent MB nanoring {Mo_{154}} (left), and the {Mo_{36}} unit (right) from transferrable building blocks. Color scheme: {Mo_1}, yellow; {Mo_2}, red; {Mo_8}, blue (central MoO_7 pentagonal bipyramid, light blue).

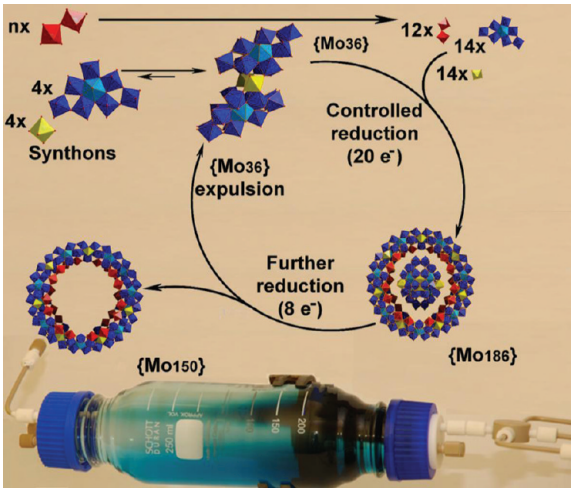

Figure 2. Scheme showing the assembly of a MB nanoring, complete with {Mo_{36}} template under continuous flow conditions. Color scheme: {Mo_1}, yellow; {Mo_2}, red; {Mo_8}, blue (central MoO_7 pentagonal bipyramid, light blue). Background shows the flow reactor setup used in our studies.

In this paper we verify, build on, and develop the results first presented by us in 2010[49] by first fully exploring the reaction parameters surrounding generation and isolation of the title compound, **1**. This is because the conditions required for isolation of **1** using the reactor reservoir and controlled flow of acid and reducing agent have been optimized, and the optimization has provided us with further information about

dx.doi.org/10.1021/ja210206z | J. Am. Chem. Soc. 2012, 134, 3816−3824

the self-assembly processes at work, so we can discuss our proposed reaction mechanism in more detail. Second, we expanded the solution-based studies using dynamic light scattering (DLS) on the crude reaction mixture from which compound **1** crystallizes, in an attempt to follow the self-assembly of the anionic molybdenum synthons and their subsequent structural evolution into the MB nanoring. In this respect it is worth mentioning that the application of DLS to solution monitoring in "real time" under flow of the MB reactant solution is unprecedented, with previous studies focusing on the vesicle-type formation and the amphiphilic properties and intermolecular interactions of MB and other polyoxometalate species.[50−52] Third, a comprehensive study of the structural and electronic properties of compound **1** was performed, not only to enable speculation of its practical applications but also to compare it with the archetypal MB rings and further establish its assignment as an essential reaction intermediate. Finally, a reanalysis of the complex structure of **1**, first presented in ref 49, is done to show how the wheel acts as an electronically deformable host, and further data regarding the host−guest complex from a series of Raman and UV/vis spectroscopic measurements are presented.

RESULTS AND DISCUSSION

A typical synthesis of a MB ring such as $Na_{35}[Mo_{150}O_{451}(OH)_5(H_2O)_{61}]\cdot xH_2O$ follows a standard "one-pot" procedure, whereby an aqueous solution of $(NH_4)_6Mo_7O_{24}\cdot 4H_2O$ is adjusted to pH 1.4−1.7 with HCl. Addition of hydrazinium dichloride powder follows, and after the mixture is kept stationary for 2−6 weeks at 15 °C, dark blue plate crystals appear as described in ref 54; however, for the most used synthesis see refs 47c and d. In the 6-week period from addition of the reducing agent to filtration and collection of the crystallized product, very little information can be gained from this experimental setup. Many questions are left unanswered: When are the necessary synthons for the ring formation generated? Are all $\{Mo_{36}\}$ clusters degraded upon the initial reduction? Do nonreduced Mo fragments recombine to re-form $\{Mo_{36}\}$? To help answer these questions, we designed a new synthetic procedure for the MB reactions, consisting of a reactor reservoir, controlled mixer, and inlet−outlet flow feeds (Figure 2). The reactor setup enabled real-time adjustment of the key experimental variables (pH, concentration of molybdate, and reducing agent concentration) that influence the reaction. Carrying out the reaction in this manner, instead of proceeding directly to crystallization of a MB ring product, resulted in the isolation of the host−guest intermediate $\{Mo_{36}\}\subset\{Mo_{150}\}$, compound **1**, as first reported by us in 2010.[49]

Crystallographic and Solid-State Studies. In addition to studies on the assembly processes of compound **1**, investigations of the physical properties of the material have been extended as well. Although the wheel-type molybdenum blue architectures are very complex, the general approach to the structural analysis and formula determination is well documented for both the wheel host[48] and the guest molecule.[54] In the case of the wheel cluster, this is a large mixed-valence molecule, and structural analysis requires the following information to allow the assignment of formula and structural details by a systematic approach that eliminates the unknown variables:

(i) Redox titration to help determine the number of reduced Mo^V centers. UV/vis spectroscopy can also help corroborate this data via analysis of the extinction coefficient for the ligand to metal charge transfer (LMCT) and intervalence charge transfer (IVCT) bands associated with the reduced Mo^V centers. Each center should contribute ca. $(5–6)\times 10^3$ L·mol^{-1}·cm^{-1} to ε.

(ii) Sodium and molybdenum flame atomic absorption spectrometry (FAAS) analysis.

(iii) Thermogravimetric analysis (TGA) to estimate the number of solvent water molecules (although this is difficult since the crystals are very highly hydrated and lose water immediately upon removal from the mother liquor).

(iv) Bond valence sum analysis to confirm the oxo and hydroxo ligands as well as to study the electron distribution over the reduced Mo^V centers.[55]

Therefore, the following analysis both presents these data and demonstrates how the structural assignment is consistent with these data. Compound **1** was determined to have the composition $Na_{22}\{[Mo^{VI}_{36}O_{112}(H_2O)_{16}]\subset[Mo^{VI}_{130}Mo^{V}_{20}O_{442}(OH)_{10}(H_2O)_{61}]\}\cdot 180H_2O$ from structural analysis, redox titration, elemental analysis, TGA, and evaluation of the bond valence sums. The overall reduction state of the wheel (20-electron-reduced) was confirmed by three independent techniques, visible spectroscopy, redox titration, and bond valence sum analysis; it is also consistent with the sodium ion elemental analysis. Compound **1** crystallizes in the space group $C2/m$ and has a unit cell of a = 29.4139(9), b = 51.1644(9), c = 30.5935(12) Å, and β = 114.979(4)° with a unit cell volume of 41.735(2) Å^3.[49] Structural solution reveals the metal-oxide nanoscale $\{Mo_{150}\}$ wheel host, which has an oval-shaped central cavity of approximately 25.0 × 21.0 Å, accommodates a $\{Mo_{36}\}$ unit. The remaining free space between the $\{Mo_{150}\}$ wheel and the $\{Mo_{36}\}$ unit is occupied by Na^+ cations, most of which bridge the two units directly through the oxo ligands on both clusters. The rest of the Na^+ cations are coordinated via oxo ligands to the $\{Mo_{36}\}$ cluster and to water molecules which form an extended network of H-bonds with the oxo ligands of the $\{Mo_{150}\}$ cluster. Finally, the coordinated water ligands on the dimeric $\{Mo^{VI}_2O_5(H_2O)_2\}^{2+}$ units located on the rim of the $\{Mo_{150}\}$ wheel (Figure 1, red polyhedra) are H-bonded to the oxo ligands of the $\{Mo_{36}\}$ cluster. The complicated network of hydrogen and coordination bonds presumably keeps the template in the optimum position for self-assembly to occur while it induces enough stability to the system and makes it possible to "trap" the transient $\{Mo_{186}\}$ species. One quarter of the molecule was found in the asymmetric unit with a number of Mo (Mo7, Mo13, Mo24) and O atoms located on special positions, that is, on the crystallographic mirror plane or C_2 axis. The related $\{Mo_{154}\}$ ring cluster has very high symmetry of D_{7d} point group.[48] Due to the two defect sites (missing four Mo atoms near the $\{Mo_{36}\}$ cluster corners), the $\{Mo_{150}\}$ cluster possesses symmetry of the C_{2h} point group. The sole mirror plane is defined by Mo7, Mo13, and Mo24 atoms; the C_2 axis is vertical to this plane and passes through the molecular center. All the Mo atoms (including those disordered) and most of the O atoms were refined anisotropically. Mo5 and Mo6, which link externally between clusters, were found partially occupied (occupancy = 0.75 each). This implies defects are partially formed at the linking positions between clusters. Na cations were identified ($d_{Na-O}\approx 2.4$ Å) and refined isotropically. Solvent water molecule sites with partial occupancy were found and included in the structure refinement. The ring-shaped anionic part of **1** (Figure 3) consists of three different building block types: $\{Mo_8\}$, $\{Mo_1\}$, and $\{Mo_2\}$.

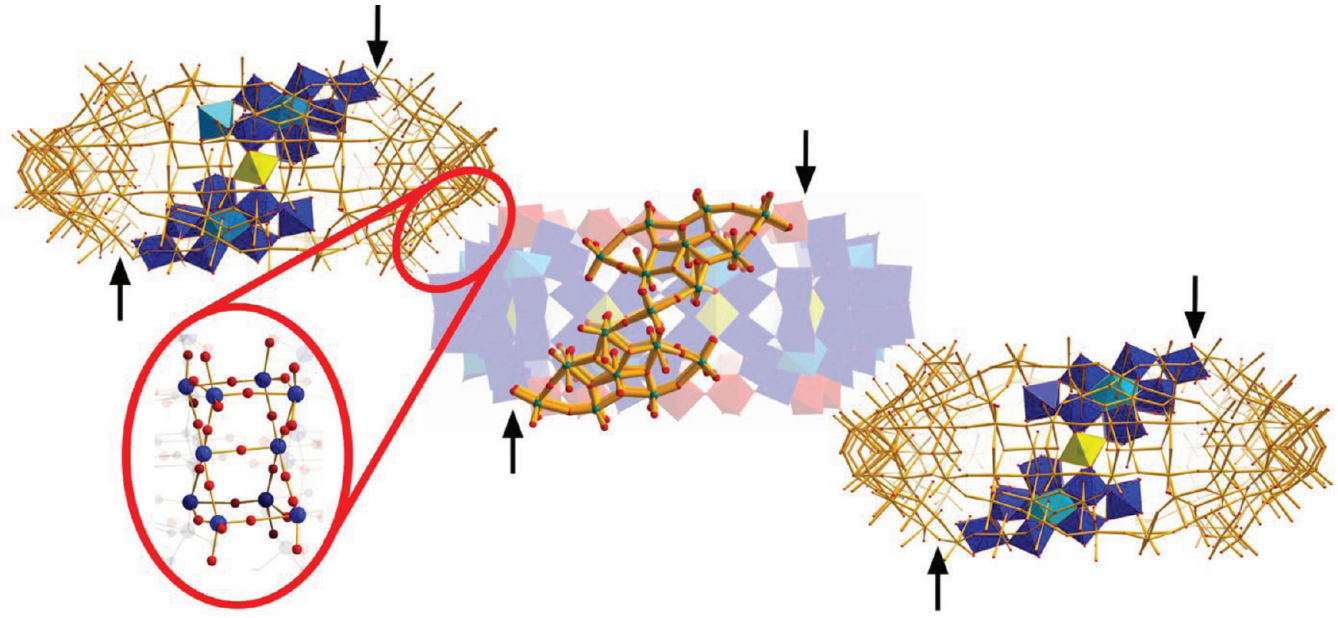

Figure 3. Polyhedral representation of the polymeric 1D chain in **1**. Sodium cations have been omitted for clarity. The MB rings are connected through five O-bridges at a distance of ~4 Å. The moieties are represented by alternating polyhedra and wire sticks, respectively, and the coloring reflects the different building block types: $\{Mo_1\}$ = yellow; $\{Mo_2\}$ = red; $\{Mo_8\}$ = blue (the pentagonal Mo center is highlighted as cyan). Black arrows point toward the defect sites of the ring.

The archetypal $\{Mo_{154}\}$ ring system[47] contains 14 of each unit, whereas the $\{Mo_{150}\}$ wheel presented here contains 14 $\{Mo_8\}$ units and 14 $\{Mo_1\}$ units but only 12 $\{Mo_2\}$ units. Furthermore the $\{Mo_{36}\}$ template can be viewed as comprising four $\{Mo_8\}$ units, two $\{Mo_1\}$ units and two $\{Mo_1\}$* (half a $\{Mo_2\}$). The $\{Mo_8\}$ unit contains a central Mo atom that has an important pentagonal bipyramidal geometry of the form $\{(Mo{=}O)O_6\}$; the seven other MoO octahedra are grouped by corner- and edge-sharing to form an $\{Mo_8\}$ fragment. The fragments arranged above and below the equatorial plane of the cluster anion are linked to each other by the oxygen atoms in this plane; 12 $\{Mo_2O_5(H_2O)_2\}^{2+}$ or $\{Mo_2\}$ units above and below the equatorial plane and 14 equatorial $\{Mo_1\}$ centers. A further characteristic of the structure of anion **1** is the large number of protons resulting from the 20 e^- reduction. A careful analysis of the bond valence sums revealed 10 singly and 60 doubly protonated oxygen atoms. The 10 equivalent O atoms, situated in the equatorial plane (Figure 3) and linking two $\{Mo_8\}$ units as well as another Mo atom that also lies in this plane, are singly protonated.

The $\{Mo_{150}\}$ ring found in compound **1** can be geometrically related to the ring-shaped $\{Mo_{154}\} \equiv [Mo_{154}O_{462}H_{14}(H_2O)_{70}]^{14-}$ parent-cluster archetype.[48] According to the classification devised to describe these MB-ring-type architectures, the formula of the $\{Mo_{150}\}$ wheel in **1** can be expressed as $[\{Mo_2\}_{12}\{Mo_8\}_{14}\{Mo_1\}_{14}]^{14-}$ with the overall formula $[Mo^{VI}_{130}Mo^{V}_{20}O_{442}(OH)_{10}(H_2O)_{61}]^{14-}$. In this case the condensation of these ring clusters results in the formation of a one-dimensional (1D) chain via the substitution of five water molecules per cluster with five O-bridges that are shared between the rings at the connectivity points (Figure 3).

Interestingly, bond valence sum (BVS)[55] calculations for the Mo centers showed a distribution pattern according to the location of the defect sites. More specifically, the area close to the defect sites consists of fully oxidized centers, while the valence reduces to the value of 5.1 along the periphery of the ring at the antipodal site (Figure 4). This type of electronic anisotropy is unprecedented in the MB family of compounds

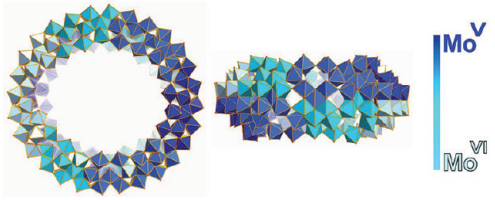

Figure 4. Top (left) and side-view (right) representation of the average BVS value distribution. Dark blue, Mo(V); light blue, Mo(VI).

since in all previously reported cases the wheels revealed 28 electrons delocalized over all 14 $\{Mo_8\}$ compartments.[56] This unique feature again reflects the transient nature of compound **1**.

Since our first effort to isolate **1**, we have managed to further optimize our setup and experimental conditions. More specifically, the optimized reaction conditions with respect to maximum yield of **1** and shortest reaction time were obtained when solutions of $Na_2MoO_4{\cdot}2H_2O$ (2.46 M, 60 mL), HCl (5.0 M, 60 mL), and $Na_2S_2O_4$ (0.19 M, 60 mL) were premixed in a cross-manifold and introduced to the reaction reservoir containing a premixed solution of K_2MoO_4 (0.2 M, 250 mL) and HNO_3 (0.4 M, 250 mL). The flow rate for the three inlet feeds was required to be between 4 and 6 mL/h, which resulted in a flow rate of 12−18 mL/h at the reservoir inlet. Flow rates outside this window yielded inferior results with respect to isolation of **1**. Slower flow rates resulted in accumulation of precipitated molybdenum salts between the cross-manifold mixer and the reservoir inlet, which blocked the flow, while higher flow rates increased the mixing vortex of the reduced molybdate feed and the acidified molybdate as it entered the reservoir, causing a uniform mixture from which $\{Mo_{36}\}$ and $\{Mo_{154-x}\}$ (where x denotes the number of defect sites in the MB ring) crystallized separately as colorless columnar crystals and dark

dx.doi.org/10.1021/ja210206z | J. Am. Chem. Soc. 2012, 134, 3816−3824

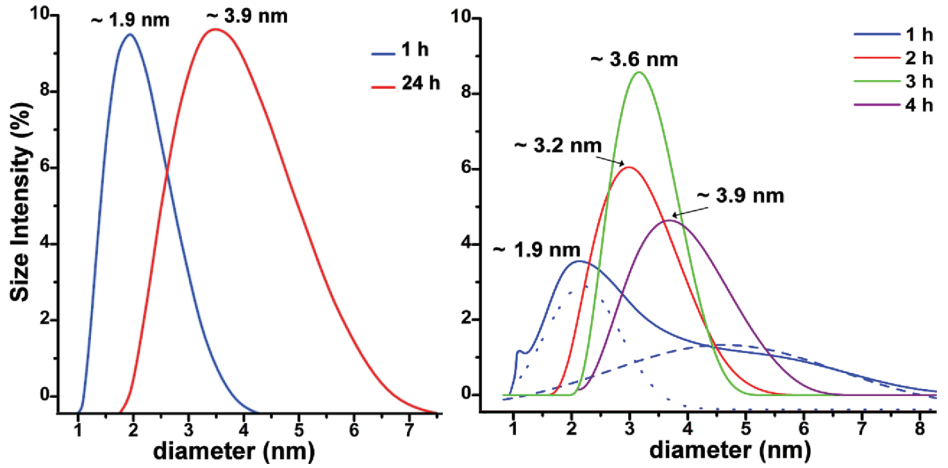

Figure 5. DLS plots of particle sizes for solutions evolving over time. (Left) Acidification of Mo solution triggers the formation of the $\{Mo_{36}\}$ unit (blue line), while upon reduction the formation of the Mo blue ring is detected (red line). (Right) Seeding the reduced acidified Mo solution with $\{Mo_{36}\}$ unit accelerates the ring formation process. Blue dotted line: Gaussian fitting for the three overlapping peaks after the first hour.

blue rhombohedral crystals, respectively. Similarly, when the ratio of the reduced molybdate volume was altered with respect to the acidified molybdate volume, both $\{Mo_{36}\}$ and $\{Mo_{154-x}\}$ again crystallized separately from the mixture; however, in this case a rough trend was observed whereby the ratio of the number of $\{Mo_{154-x}\}$ to $\{Mo_{36}\}$ crystals increased with the volume of reduced molybdate added. This showed that the theoretical ratio of $\{Mo_{36}\}$ and $\{Mo_{154-x}\}$ from the reactant feeds was reflected in the product mixture; therefore, for the 1:1 host–guest complex to form, conditions reflecting this ratio would have to be met by the two molybdate sources. For the optimized conditions previously stated and with the assumptions of 100% conversion of acidified molybdate to $\{Mo_{36}\}$, 100% conversion of reduced molybdate feed to $\{Mo_{150}\}$, and that the volume of $\{Mo_{150}\}$ solution entering the reactor reservoir displaces the same volume of $\{Mo_{36}\}$ solution initially inside the reservoir, we calculated theoretical values of 0.88 and 0.98 mmol of $\{Mo_{36}\}$ and $\{Mo_{150}\}$, respectively. This theoretical ratio based simply on the molar concentrations of molybdenum from each source is therefore 1:1.1 and could offer a reasonable explanation as to why the complex forms only under these specific conditions.

The setup of a concentration gradient by controlled addition of reduced acidified molybdate to the acidified molybdate solution, which promotes the formation of $\{Mo_{36}\}$ species, enabled the isolation of the $\{Mo_{36}\}\subset\{Mo_{150}\}$ host–guest complex but did not prove the templating effect of $\{Mo_{36}\}$ under conditions favoring formation of the 28-electron-reduced empty MB rings $\{Mo_{154-x}\}$. A comparative experiment was therefore set up, where in one reactor the acidified molybdate solution was directly reduced, and in the other, the reduced acidified molybdate solution was flowed into a reactor containing additional acidified molybdate. After 1 day, the flow reactor had yielded gram quantities of the $\{Mo_{154-x}\}$ product, whereas the batch reaction required an additional 3–4 days to yield comparable quantities of the product. In the flow reactor, the incoming prereduced acidified molybdate does not degrade the $\{Mo_{36}\}$ already present in the reactor, thus allowing it to template the MB ring formation. In the batch reactor, the $\{Mo_{36}\}$ is reduced by direct addition of the reducing agent, and without the $\{Mo_{36}\}$ template in the solution, the assembly of the MB ring product takes much longer.

Time-Resolved Dynamic Light Scattering Studies. In an effort to authenticate the template effect the $\{Mo_{36}\}$ has on MB ring formation, we hypothesized that differences in particle size for the $\{Mo_{36}\}$ and $\{Mo_{154-x}\}$ species could be measured by DLS and used to directly follow the self-assembly and structural evolution of the solutions directly. When a solution of K_2MoO_4 (0.2 M) was acidified with equal volumes of HNO_3 (0.4 M), emulating the conditions used for the flow reactor, a DLS plot showed the presence of nanoparticles with a hydrodynamic diameter of 1.9 nm. From the crystallographic studies of compound **1**, it is known that the dimensions of the template cluster are 1.3 × 1.3 × 1.7 nm, therefore when considering the associated cations and primary solvation sphere are considered, a size of ~1.9 nm is in good agreement with this structure. The peak at ~1.9 nm was observed immediately after mixing of the two solutions and remained for a period of 6 h (see Figure 5, blue line, and Supporting Information), during which time the solid $\{Mo_{36}\}$ material crystallized out of the solution (confirmed by unit cell checks). In another set of experiments, a reduced molybdate solution (2.46 M Na_2MoO_4 + 0.19 M $Na_2S_2O_4$) was acidified (5.0 M HCl, 1:1:1 by volume) whereby the formation of MB rings was observed after 24 h, indicated by a peak in the region of 3.7–4.1 nm, which is again in good agreement with the diameter of the ring including the hydration/ionic sphere (Figure 5, red line). Upon standing at room temperature, the $\{Mo_{154}\}$ ring crystallized after 7 days (confirmed by unit cell checks). Similarly, all members of the MB family of rings (Mo_{138}–Mo_{154}),[48,53] which can be synthesized as a function of the pH value and give ring-shaped species, are accompanied by a peak in the same region of sizes (3.7–4.1 nm). When an aliquot of the prepared $\{Mo_{36}\}$ solution (9 mL) was added to a premixed solution of the reduced acidified molybdate (5.0 M HCl, 2.46 M $Na_2MoO_4{\cdot}2H_2O$, and 0.19 M $Na_2S_2O_4$, 41 mL, 1:1:1 by volume) a peak at 3.7–4.1 nm appeared after only 4 h, indicating highly accelerated formation of the wheel structure around the template in agreement with the proposed mechanism.

After a 24 h period, much larger aggregates in the region of 100 nm can be detected. These larger particle sizes are caused by the inherent nature of the Mo blue rings to form macromolecular architectures such as 1D chains and/or blackberry formations in solution.[48,57] The appearance of these peaks of larger particle size in addition to those at 3.7–4.1 nm is

dx.doi.org/10.1021/ja210206z | J. Am. Chem. Soc. 2012, 134, 3816–3824

therefore unavoidable when observing a continuously evolving complex reaction mixture solution such as this. The dramatic decrease in the length of time taken to observe the nanowheel structure when the MB synthons are created with additional $\{Mo_{36}\}$ (4 h), compared to without (24 h), offers additional proof of the catalytic template effect of the $\{Mo_{36}\}$ unit during formation of the larger wheel cluster. DLS measurements were further used to probe the dual role of the $\{Mo_{36}\}$ cluster, as both template and molybdenum source for the pentagonal wheel building blocks as proposed in the original mechanism.[49] When equal volumes of K_2MoO_4 (0.2 M) and HNO_3 (0.4 M) were mixed, a peak stable over time was observed at 1.7–1.9 nm in the DLS plots, indicative of the $\{Mo_{36}\}$ template as seen previously. When the reducing agent $Na_2S_2O_{4(s)}$ (10 mol % with respect to Mo) was added directly to the template solution and the pH was readjusted to ~1.7 by addition of concentrated HCl, the peak at 1.7–1.9 nm disappeared and no peaks for particle sizes under 10 nm were observed during the first 2 h. After this time, a peak at 0.9 nm was observed, indicating the re-formation of nanometer-sized particles while after 3–4 h a peak at 3.6–3.9 nm was observed, indicating the formation of nanowheel-sized structures (Figure 6). Addition of the reducing

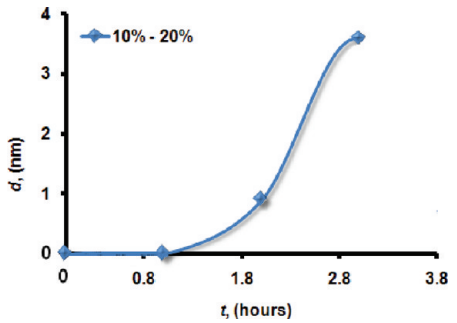

Figure 6. DLS plot of particle's diameter for a partially reduced Mo solution as a function of time.

agent directly to the template solution initially causes the discrete $\{Mo_{36}\}$ species to break down into small building units, acting as internal feedstock for the generation of the reduced $\{Mo_8\}$ building units. Given time, the system re-equilibrates to form both the MB synthons and $\{Mo_{36}\}$ template, which then combine in the formation of the template wheel, followed by ejection of the template to produce the MB ring final product. After 4–5 h the concentration of nanowheel products increases and only large aggregate structures appear in the DLS plots, making it difficult to ascertain information regarding the reaction composition beyond this time. When the amount of reducing agent added exceeds the value of 20% (with respect to Mo), over-reduction of the molybdenum centers takes place and large polymeric aggregations (10–100 nm) are formed almost instantly (unidentified polymeric molybdenum oxide phase). When the added amount of reducing agent is increased to 25%, 50%, and 75% (with respect to Mo), faster formation of polymeric molybdenum oxide species can be detected at 5, 3, and 2 h, respectively (see Supporting Information). Consequently, the aforementioned aggregations, due to over-reduction of the molybdate solution, prevent the evolution of the reaction mixture in the desired direction of formation of MB rings.

Finally, by using a continuous-flow setup connected directly to the DLS particle sizer, changes with respect to particle size within the reaction mixture could be observed as a function of the reagent feed composition (Figure 7). During the first time period (Figure 7a), the material flowing through the DLS flow

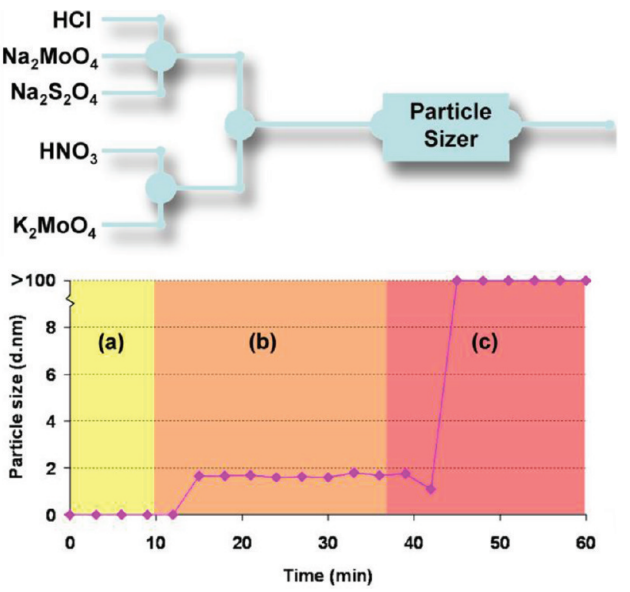

Figure 7. Monitoring molecular evolution in the flow reactor by leading the reaction mixture through a DLS flow cell. Top: Schematic of physical connectivity of the feed stocks and reagent mixing chambers. (a) Area shaded yellow shows time period where only K_2MoO_4 feed stock was flowing. (b) Area shaded orange shows time period where both K_2MoO_4 and HNO_3 feed stocks were flowing. (c) Area shaded red shows time period where all five reagents were flowing. Note that discrete molecular clusters are not observed here as the rate of MB nanowheel formation is much slower than the residence time between mixing and the DLS flow cell. Pump flow rates for each feed were set at a constant 3 mL/h, and reagent concentrations were the same as those used in the original synthesis.[49]

cell was composed purely of 0.2 M K_2MoO_4 and therefore showed no peaks correlating to nanoparticle formation. During the second time period (Figure 7b), a flow of 0.4 M HNO_3 was started in addition to the 0.2 M K_2MoO_4. The material flowing through the DLS flow cell then gave a signal at 1.7–1.9 nm, which was consistent with the formation of the $\{Mo_{36}\}$ template species observed during the batch reactions. During the final time period (Figure 7c), the solutions of 5.0 M HCl, 2.46 M Na_2MoO_4, and 0.19 M $Na_2S_2O_4$ were fed into the flow network. Unfortunately a direct conversion of the template-sized particles to nanowheel-sized particles was not observed; instead peaks at >100 nm, thought to be aggregations of Mo-based species, were seen. This, however, was not entirely unexpected, considering the fastest rate of formation of the MB nanowheel observed from the previous reactions was 4 h and the residence time for the reaction mixture between the point of mixing and the DLS flow cell was calculated as only 4 min (see Supporting Information for dimensions and calculations).

Spectroscopic and Stability Studies. Raman studies were conducted on the $\{Mo_{36}\}$ template, the 28-electron-reduced $\{Mo_{150}\}$ empty wheel, and the $\{Mo_{36}\}\subset\{Mo_{150}\}$ complex (see Figure 8). Analysis of the spectra reveals similarities and distinctions between all three materials in the solid state. As expected, the Raman spectrum of compound **1** can be regarded as an amalgamation of the individual spectra of $\{Mo_{36}\}$ and $\{Mo_{150}\}$, respectively. The main features of the spectra are

dx.doi.org/10.1021/ja210206z | J. Am. Chem. Soc. 2012, 134, 3816–3824

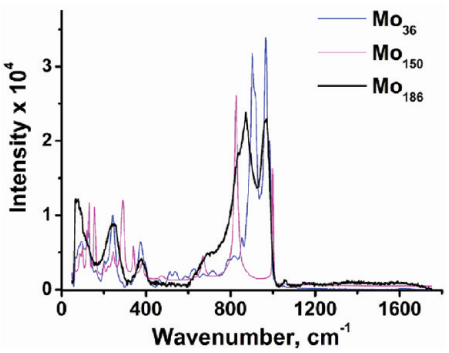

Figure 8. Overlaid Raman spectra for $\{Mo_{36}\}$ template, $\{Mo_{36}\}\subset\{Mo_{150}\}$ complex, and $\{Mo_{150}\}$ empty wheel cluster.

located in the region 800−1000 cm^{-1} due to Mo═O (sym/asym) at higher frequencies and to Mo−O−Mo (sym) at lower frequencies.[58] Moreover, a minor broadening of the bands was observed due to the existence of an extensive network of hydrogen bonds and sodium-based salt bridges within the core of the architecture, which are partially responsible for keeping the $\{Mo_{36}\}$ at the center of the cavity. Similar behavior has been observed before; where proton-induced polarizabilities contribute to the electron-based ones, causing a broader distribution of accessible energy levels.[25,59,60]

The oxidative stability of the $\{Mo_{36}\subset Mo_{150}\}$ complex was also investigated in a comparative experiment with the 28-electro-reduced $\{Mo_{154}\}$ empty wheel by electronic absorbance spectroscopy (Figure 9). Both materials exhibit absorbance maxima at

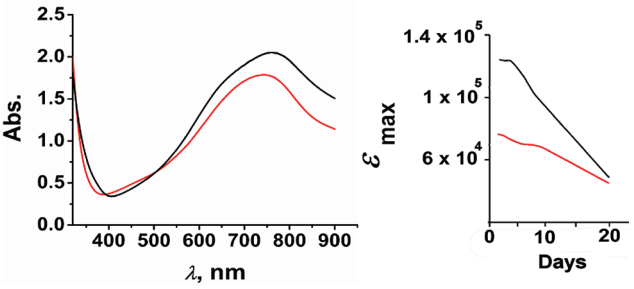

Figure 9. (Left) Electronic absorbance spectra for (black line) $\{Mo_{150}\}$ and (red line) $\{Mo_{186}\}$. (Right) Change of absorption coefficients over a period of 20 days.

748 nm due to LMCT and IVCT; the initial extinction coefficients differ between the two compounds because of the difference in the number of electrons that reside in the $\{Mo_8\}$ compartments of $\{Mo_{150}\}$ and $\{Mo_{154}\}$ wheel, 20 and 28, respectively, where each Mo^V center has been calculated to contribute ca. 5000 $L{\cdot}mol^{-1}{\cdot}cm^{-1}$ to the extinction coefficient.[49,61] As can be seen from the two sets of spectra, the Mo^V centers in both compounds are susceptible to oxidation when they are left to stand in solutions exposed to air. An interesting observation is the rate at which $\{Mo_{36}\}\subset\{Mo_{150}\}$ is oxidized in comparison to $\{Mo_{154}\}$; the relative rate of oxidation of $\{Mo_{36}\}\subset\{Mo_{150}\}$ appears to be much faster than that of $\{Mo_{154}\}$ during the first three days. The above observation suggests that the $\{Mo_{150}\}$ ring is much easier to oxidize than the initially stable 28-electron configuration in the $\{Mo_{154}\}$ ring.

CONCLUSIONS

In summary, an optimized synthetic procedure of **1**, $\{Mo_{36}\}\subset\{Mo_{150}\}$, followed by a detailed structural analysis has been reported. Furthermore, application of DLS as a tool to directly follow the solution generation of a metal oxide nanoscale wheel architecture has been demonstrated for the first time. The distinction in size between the $\{Mo_{36}\}$ template and the $\{Mo_{36}\}\subset\{Mo_{150}\}$, complex and $\{Mo_{150}\}$ ring allowed the identification of these species in the reaction mixture solution and monitored their evolution over time, thus providing further information to substantiate and elaborate the formation mechanism originally proposed for this important family of compounds. Additionally, a comparative stability study of compound **1** and the archetypal $\{Mo_{150}\}$ ring was carried out by visible absorbance spectroscopy, and Raman spectroscopy reflected the structural correlation between them. The information obtained here demonstrates the value of the DLS technique in combination with X-ray diffraction and spectroscopic studies when trying to understand the self-assembly of such intricate nanosized molecular metal oxide systems. Although the qualitative data obtained do not allow comprehensive kinetic studies at this stage, it brings us one step closer to understanding the formation of complicated systems like the MBs in solution. It is our aim to use these techniques to follow the assembly of other self-assembled chemical systems in solution that will open the door to further understanding and finally control of such complex self-assembly processes. The characterization of the "bottom-up" designed nanosized species in solution will also overcome the problems associated with product crystallization and isolation and will ultimately unveil the true potential of solution-processable nanosized metal oxides to be exploited in the manufacture of novel materials and molecular devices with engineered functionality.

EXPERIMENTAL SECTION

Instruments and Materials. All starting materials were commercially available (reagent grade) and were used as supplied from Sigma−Aldrich Chemical Co. without further purification. The particle sizes were determined on a Malvern Instruments Zetasizer Nano ZS instrument at 25 °C. The instrument uses a 4 mW He−Ne laser operating at a wavelength of 633 nm and incorporates non-invasive backscatter optics (NIBS). The measurements were performed at a detection angle of 173°, and the measurement position within the disposable plastic cuvettes was automatically determined by the software. Due to the NIBS fiber optic system, the particle sizer can accurately determine hydrodynamic particle sizes down to 0.6 nm diameter (0.3 nm radius).[62,63] All measurements were performed multiple times (>3) to ensure the consistency of the results.

Raman Spectroscopy. Raman spectra were recorded on an HR800 spectrometer in conjunction with HeNe 20 mW (λ = 532 nm) laser with crystalline solid substances.

Single-Crystal X-ray Diffraction. Crystal data and structure refinement for compound **1**: $H_{524}Mo_{186}Na_{22}O_{821}$, M_w = 32 014.8 $g{\cdot}mol^{-1}$; a blue rod-shaped crystal (0.09 × 0.05 × 0.02 mm) was analyzed with an Oxford Diffraction Gemini Ultra diffractometer using Cu Kα radiation (λ = 1.541 84 Å) at 150(2) K. Monoclinic, space group *C*2/*m*, *a* = 29.4139(9), *b* = 51.1644(9), *c* = 30.5935(12) Å, and β = 114.979(4)° with a unit cell volume of 41.735(2) $Å^3$, *Z* = 2, ρ = 2.548 $g{\cdot}cm^{-3}$, μ(Cu Kα) = 23.245 mm^{-1}, *F*(000) = 30 292, 69 631 reflections measured, of which 23 958 are independent, 1879 refined parameters, *R*1 = 0.0757, w*R*2 = 0.2177. CSD reference 380343 (data available from CrysDATA@FIZ-Karlsruhe.de).

Visible Spectroscopy. Visible spectra were collected on a Shimadzu PharmaSpec UV-1700 UV−vis spectrophotometer in transmission mode by use of quartz cuvettes with 1.0 cm optical path length.

dx.doi.org/10.1021/ja210206z | J. Am. Chem. Soc. 2012, 134, 3816−3824

General Synthetic Procedure for Compound 1. The following solutions were prepared in deionized and degassed H_2O as follows: Solution A: 60 mL of (2.46 M) $Na_2MoO_4{\cdot}2H_2O$; Solution B: 60 mL of (5.0 M) HCl; Solution C: 60 mL of (0.19 M) $Na_2S_2O_4$; Solution D: 250 mL of (0.2 M) K_2MoO_4; Solution E: 250 mL of (0.4 M) HNO_3. Solutions A, B, and C reacted in the mixing chamber at a flow rate of 4−6 mL/h. The chamber's output entered into a 500 mL reactor that contained a mixture of solution D and E. Tiny blue rod-shaped crystals appeared within 24 h in the reactor under flow conditions (see Figure 1). Diffraction-quality crystals begin to form after 2 days upon standing. Yield after 3 days = 5.0 g (28.20% based on Mo).

Dynamic Light Scattering Sample Preparations. The Zetasizer Nano laser-light-scattering spectrometer (Malvern) was equipped with a He−Ne laser with a wavelength of 633 nm. DLS measured the intensity−intensity time correlation functions at 20 °C. The correlation functions from DLS were analyzed via the general algorithm provided by the Zetasizer software. For comparative results, the DLS samples were prepared at at the same concentrations used in the original synthetic procedure reported for compound **1** (see Results and Discussion for an optimized procedure).[49] To minimize the problems associated with aggregation and crystallization, all samples were twice filtered through 0.45 μm and then 0.22 μm syringe filters immediately prior to each measurement. For solutions of $\{Mo_{36}\}$ template, K_2MoO_4 (0.2 M) was acidified with an equal volume of HNO_3 (0.4 M); the pH of the resultant solution should be ∼1.7, and small white crystals begin to crystallize after 2−3 h. For solutions of the reduced acidified molybdate, 0.19 M $Na_2S_2O_4$ was added to an acidified (5.0 M HCl) molybdate solution (2.46 M $Na_2MoO_4{\cdot}2H_2O$), 1:1:1 by volume. For solutions of reduced acidified molybdate doped with the $\{Mo_{36}\}$ template, the individual solutions were prepared as previously described and mixed in the specified ratios after standing for no longer than 1−2 min. Intensity plots are number, volume, or intensity plotted against the size (diameter in nanometers) of the measured particle in solution.

■ ASSOCIATED CONTENT

Supporting Information

Additional text and seven figures showing sample preparation details, DLS experimental details, analyses, and plots, and electronic absorbance spectroscopy experimental details and data (PDF); structural information (CIF). This material is available free of charge via the Internet at http://pubs.acs.org/.

■ AUTHOR INFORMATION

Corresponding Author

Lee.Cronin@glasgow.ac.uk

Notes

The authors declare no competing financial interest.

■ ACKNOWLEDGMENTS

This work was supported by the EPSRC, University of Glasgow, and WestCHEM.

■ REFERENCES

(1) (a) Lehn, J.-M. *Science* **2002**, *295*, 2400−2403. (b) Whitesides, G. M.; Boncheva, M. *Proc. Natl. Acad. Sci. U.S.A.* **2002**, *99*, 4769−4774. (c) Fyfe, M. C. T.; Stoddart, J. F. *Acc. Chem. Res.* **1997**, *30*, 393−401.

(2) (a) Whitesides, G. M.; Grzybowski, B. *Science* **2002**, *295*, 2418−2421. (b) Wu, J.; Leung, K. C.-F.; Stoddart, J. F. *Proc. Natl. Acad. Sci. U.S.A.* **2007**, *104*, 17266−17271.

(3) Inokuma, Y.; Kawano, M.; Fujita, M. *Nat. Chem.* **2011**, *3*, 349−358.

(4) (a) Matsuda, R.; Tsujino, T.; Sato, H.; Kubota, Y.; Takata, M.; Kitagawa, S. *Chem. Sci.* **2010**, *1*, 315−321. (b) Furukawa, H.; Ko, N.; Go, Y. B.; Aratani, N.; Choi, S. B.; Choi, E.; Yazaydin, A. O.; Snurr, R. Q.; O'Keeffe, M.; Kim, J.; Yaghi, O. M. *Science* **2010**, *329*, 424−428.

(5) Imai, H.; Akutagawa, T.; Kudo, F.; Ito, M.; Toyoda, K.; Noro, S.; Cronin, L.; Nakamura, T. *J. Am. Chem. Soc.* **2009**, *131*, 13578−13579.

(6) Tasiopoulos, A. J.; Vinslava, A.; Wernsdorfer, W.; Abboud, K. A.; Christou, G. *Angew. Chem., Int. Ed.* **2004**, *43*, 2117−2121.

(7) Takashima, Y.; Martínez, V. M.; Furukawa, S.; Kondo, M.; Shimomura, S.; Uehara, H.; Nakahama, M.; Sugimoto, K.; Kitagawa, S. *Nat. Commun.* **2011**, *2*, 168−175.

(8) Ohara, K.; Kawano, M.; Inokuma, Y.; Fujita, M. *J. Am. Chem. Soc.* **2010**, *132*, 30−31.

(9) Holliday, B. J.; Mirkin, C. A. *Angew. Chem., Int. Ed.* **2001**, *40*, 2022−2043.

(10) Sato, S.; Iida, J.; Suzuki, K.; Kawano, M.; Ozeki, T.; Fujita, M. *Science* **2006**, *313*, 1273−1276.

(11) Mal, P.; Breiner, B.; Rissanen, K.; Nitschke, J. R. *Science* **2009**, *324*, 1697−1699.

(12) Baxter, P. N. W. In *Comprehensive Supramolecular Chemistry*; Atwood, J. L., Davies, J. E. D., MacNicol, D. D., Vögtle, F., Eds.; Pergamon/Elsevier: New York, 1996; Vol. 7, pp 9165−211.

(13) Kreickmann, T.; Diedrich, C.; Pape, T.; Huynh, H. V.; Grimme, S.; Hahn, F. E. *J. Am. Chem. Soc.* **2006**, *128*, 11808−11819.

(14) Caulder, D. L.; Raymond, K. N. *Angew. Chem., Int. Ed. Engl.* **1991**, *36*, 1439−1442.

(15) Dietrich-Buchecker, C.; Colasson, B. X.; Sauvage, J. P. In *Templates in Chemistry II*; Springer-Verlag: Berlin: 2005; Vol. *249*, pp 261−283.

(16) Matsuda, R.; Kitaura, R.; Kitagawa, S.; Kubota, Y.; Belosludov, R. V.; Kobayashi, T. C.; Sakamoto, H.; Chiba, T.; Takata, M.; Kawazoe, Y.; Mita, Y. *Nature* **2005**, *436*, 238−241.

(17) Chae, H. K.; Siberio-Pérez, D. Y.; Kim, J.; Go, Y.; Eddaoudi, M.; Matzger, A. J.; O'Keeffe, M.; Yaghi, O. M. *Nature* **2004**, *424*, 523−527.

(18) Deng, Z.; Schulz, O.; Lin, S.; Ding, B.; Liu, X.; Wei, X.; Ros, R.; Yan, H.; Liu, Y. *J. Am. Chem. Soc.* **2010**, *132*, 5592−5593.

(19) Franzman, M. A.; Schlenker, C. W.; Thompson, M. E.; Brutchey, R. L. *J. Am. Chem. Soc.* **2010**, *132*, 4060−4061.

(20) Lee, D. C.; Pietryga, J. M.; Robel, I.; Werder, D. J.; Schaller, R. D.; Klimov, V. I. *J. Am. Chem. Soc.* **2009**, *131*, 3436−3437.

(21) Setua, P.; Pramanik, R.; Sarkar, S.; Ghatak, C.; Das, S. K.; Sarkar, N. *J. Phys. Chem. B* **2010**, *114*, 7557−7564.

(22) (a) Müller, A.; Beckmann, E.; Bögge, H.; Schmidtmann, M.; Dress, A. *Angew. Chem., Int. Ed.* **2002**, *41*, 1162−1167. (b) Müller, A.; Botar, B.; Das, S. K.; Bögge, H.; Schmidtmann, M.; Merca, A. *Polyhedron* **2004**, *23*, 2381−2385.

(23) Cronin, L. High Nuclearity Polyoxometalate Clusters. In *Comprehensive Coordination Chemistry II*; McLeverty, J. A., Meyer, T. J., Eds.; Elsevier Publishers: Amsterdam, 2004; Vol.7, pp 1−57.

(24) (a) Gao, J.; Yan, J.; Mitchell, S. G.; Miras, H. N.; Boulay, A. G.; Long, D.-L.; Cronin, L. *Chem. Sci.* **2011**, *2*, 1502−1508. (b) Miras, H. N.; Ochoa, M. N. C.; Long, D.-L.; Cronin, L. *Chem. Commun.* **2010**, *46*, 8148−8150. (c) Miras, H. N.; Yan, J.; Long, D.-L.; Cronin, L. *Angew. Chem.* **2008**, *47*, 8420−8423.

(25) Pope, M. T., Müller, A., Eds. *Polyoxometalate Chemistry: From Topology via Self-Assembly to Applications*; Kluwer Academic Publishers: Dordrecht, The Netherlands, 2001.

(26) Yamase, T., Pope, M. T., Eds. *Polyoxometalate Chemistry for Nanocomposite Design*; Kluwer Academic/Plenum Publishers: New York, 2002.

(27) Borrás-Almenar, J. J., Coronado, E., Müller, A., Pope, M., Eds. *Polyoxometalate Molecular Science*; Kluwer Academic Publishers: Dordrecht, The Netherlands, 2003.

(28) Ritchie, C.; Ferguson, A.; Nojiri, H.; Miras, H. N.; Song, Y.-F.; Long, D.-L.; Burkholder, E.; Murrie, M.; Kögerler, P.; Brechin, E. K.; Cronin, L. *Angew. Chem., Int. Ed.* **2008**, *47*, 5609−5612.

(29) Nellutla, S.; van Tol, J.; Dalal, N. S.; Bi, L.-H.; Kortz, U.; Keita, B.; Nadjo, L.; Khitrov, G. A.; Marshall, A. G. *Inorg. Chem.* **2005**, *44*, 9795−9806.

(30) Zeng, H. D.; Newkome, G. R.; Hill, C. L. *Angew. Chem., Int. Ed.* **2000**, *39*, 1772−1774.

(31) Ogliaro, F.; de Visser, S. P.; Cohen, S.; Sharma, P. K.; Shaik, S. *J. Am. Chem. Soc.* **2002**, *124*, 2806−2817.

(32) Jiang, C.; Lesbani, A.; Kawamoto, R.; Uchida, S.; Mizuno, N. *J. Am. Chem. Soc.* **2006**, *128*, 14240−14241.
(33) (a) Pradeep, C. P.; Long, D. L.; Cronin, L. *Dalton Trans.* **2010**, *39*, 9443−9457. (b) Long, D.-L.; Tsunashima, R.; Cronin, L. *Angew. Chem., Int. Ed.* **2010**, *49*, 1736−175.
(34) (a) Wilson, E. F.; Miras, H. N.; Rosnes, M. H.; Cronin, L. *Angew. Chem., Int. Ed.* **2011**, *50*, 3720−3724. (b) Rosnes, M. H.; Musumeci, C.; Pradeep, C. P.; Mathieson, J. S.; Long, D.-L.; Song, Y.-F.; Pignataro, B.; Cogdell, R.; Cronin, L. *J. Am. Chem. Soc.* **2010**, *132*, 15490−15492.
(35) Rogers, A.; Mitchell, F. H. *J. Am. Chem. Soc.* **1900**, *22*, 350−351.
(36) (a) Müller, A.; Meyer, J.; Krickemeyer, E.; Diemann, E. *Angew. Chem. Int . Ed. Engl.* **1996**, *35*, 1206−1208. (b) Müller, A.; Serain, C. *Acc. Chem. Res.* **2000**, *33*, 2−10.
(37) Müller, A.; Krickemeyer, E.; Bögge, H.; Schmidtmann, M.; Peters, F.; Menke, C.; Meyer, J. *Angew. Chem., Int. Ed.* **1997**, *36*, 483−486.
(38) Müller, A.; Koop, M.; Bögge, H.; Schmidtmann, M.; Beugholt, C. *Chem. Commun.* **1998**, 1501−1502.
(39) Müller, A.; Kögerler, P. *Coord. Chem. Rev.* **1999**, *182*, 3−17.
(40) (a) Müller, A.; Krickemeyer, E.; Bögge, H.; Schmidtmann, M.; Peters, F. *Angew. Chem., Int. Ed.* **1998**, *37*, 3360−3363. (b) Schäffer, C.; Todea, A. M.; Gouzerh, P.; Müller, A. *Chem. Commun.* **2012**, *48*, 350−352.
(41) Müller, A.; Shah, S. Q. N.; Bögge, H.; Schmidtmann, M.; Kögerler, P.; Hauptfleisch, B.; Leiding, S.; Wittler, K. *Angew. Chem., Int. Ed.* **2000**, *39*, 1614−1616.
(42) Müller, A.; Roy, S. *Coord. Chem. Rev.* **2003**, *245*, 153−166.
(43) Kroto, H. W.; Heath, J. R.; O'Brien, S. C.; Curl, R. F.; Smalley, R. E. *Nature* **1985**, *318*, 162−163.
(44) Miras, H. N.; Wilson, E. F.; Cronin, L. *Chem. Commun.* **2009**, 1297−1311.
(45) Liu, T. *Langmuir* **2010**, *26*, 9202−9213.
(46) Roy, S.; Planken, K. L.; Kim, R.; Mandele, D. v. d.; Kegel, W. K. *Inorg. Chem.* **2007**, *46*, 8469−8471.
(47) (a) Müller, A.; Das, S. K.; Fedin, V. P.; Krickemeyer, E.; Beugholt, C.; Bögge, H.; Schmidtmann, M.; Hauptfleisch, B. *Z. Anorg. Allg. Chem.* **1999**, *625*, 1187−1192. (b) Müller, A.; Serain, C. *Acc. Chem. Res.* **2000**, *33*, 2−10. (c) Müller, A.; Das, S. K.; Krickemeyer, E.; Kuhlmann, C. (checked by Sadakane, M., Dickman, M. H., Pope, M. T.) *Inorganic Syntheses 34*; Shapley, J. R., Ed.; Wiley: New York, 2004; pp 191−200. (d) Cronin, L.; Diemann, E.; Müller, A. In *Inorganic Experiments*; Woollins, J. D., Ed.; Wiley−VCH: Weinheim, Germany, 2003; pp 340−346.
(48) Müller, A.; Krickemeyer, E.; Bögge, H.; Schmidtmann, M.; Beugholt, C.; Das, S. K.; Peters, F. *Chem.—Eur. J.* **1999**, *5*, 1496−1502.
(49) Miras, H. N.; Cooper, G. J. T.; Long, D.-L.; Bögge, H.; Müller, A.; Streb, C.; Cronin, L. *Science* **2010**, *327*, 72−74.
(50) Pradeep, C. P.; Misdrahi, M. F.; Li, F.-Y.; Zhang, J.; Xu, L.; Long, D.-L.; Liu, T.; Cronin, L. *Angew. Chem., Int. Ed.* **2009**, *48*, 8309−8313.
(51) Kistler, M. L.; Liu, T.; Gouzerh, P.; Todea, A. M.; Müller, A. *Dalton Trans.* **2009**, 5094−5100.
(52) Zhang, J.; Song, Y.-F.; Cronin, L.; Liu, T. *J. Am. Chem. Soc.* **2008**, *130*, 14408−14409.
(53) Shishido, S.; Ozeki, T. *J. Am. Chem. Soc.* **2008**, *130*, 10588−10595.
(54) Long, D.-L.; Streb, C; Kögerler, P; Cronin, L. *J. Cluster Sci.* **2006**, *17*, 257−266.
(55) Brown, I. D. in *Structure and Bonding in Crystals*; O'Keefe, M., Navrotdsky, A., Eds.; Academic Press: New York, 1981; Vol. *II*, p 1.
(56) Zhong, D.; Sousa, F. L.; Müller, A.; Chi, L.; Fuchs, H. *Angew. Chem., Int. Ed.* **2011**, *50*, 7018−7021.
(57) Liu, T.; Diemann, E.; Li, H.; Dress, A. W. M.; Müller, A. *Nature* **2003**, *426*, 59−62.
(58) Tytko, K. H.; Schönfeld, B.; Buss, B.; Glemser, O. *Angew. Chem., Int. Ed.* **1973**, *12*, 330−332.
(59) Librovich, N. B.; Sakun, V. P.; Sokolov, N. D. *Chem. Phys.* **1979**, *39*, 351−366.
(60) Abramczyk, H. *Chem. Phys.* **1990**, *144*, 305−318.
(61) Buckley, R. I.; Clark, R. J. H. *Coord. Chem. Rev.* **1985**, *65*, 167−218.
(62) Pradeep, C. P.; Long, D.-L.; Streb, C.; Cronin, L. *J. Am. Chem. Soc.* **2008**, *130*, 14946−14947.
(63) Kaszuba, M.; McKnight, D.; Connah, M. T.; McNeil-Watson, F. K.; Nobbmann, U. *J. Nanopart. Res.* **2008**, *10*, 823−829.